EARTH SURFACE PROCESSES AND LANDFORMS
Earth Surf. Process. Landforms (2013)

Published online in Wiley Online Library
(wileyonlinelibrary.com) DOI: 10.1002/esp.3470

Tree root mounds and their role in transporting soil on forested landscapes

Benjamin S. S. Hoffman[1] and Robert S. Anderson[1,2]*
[1] Institute of Arctic and Alpine Research (INSTAAR), University of Colorado, Boulder, CO, USA
[2] Department of Geological Sciences, University of Colorado, Boulder, CO, USA

Received 17 January 2013; Revised 25 June 2013; Accepted 15 July 2013

*Correspondence to: Robert S. Anderson, Institute of Arctic and Alpine Research (INSTAAR), University of Colorado, Boulder, CO, USA. E-mail: Robert.S.Anderson@colorado.edu

ESPL
Earth Surface Processes and Landforms

ABSTRACT: The growth and decay of tree roots can stir and transport soil. This is one process that contributes to the mass-movement of soil on hillslope. To explore the efficiency of this process, we document the mounding of soil beside Ponderosa and Lodgepole pine trees in the forests that dominate the mid-elevations of Colorado's Boulder Creek watershed. Mounds are best expressed around Ponderosa pines, reaching vertical displacements above the far-field slopes of order 10–20 cm, fading into the slope by roughly 100 cm distance from the trunks with common diameters of 30 cm. Positive mounding occurs on all sides of trees on slopes, indicating that the mounding is not attributable to deflection of a creeping flow of soil around the tree, but rather to the insertion of root volume on all sides in the subsurface. Mounding is commonly asymmetric even on cross-slope profiles. Significant variation in the mound sizes results in no clear relationship between tree diameter and root volume displaced. These observations motivated the development of a discrete element model of tree root growth using the LIGGGHTS model, in which grains we specified to be 'root cells' were allowed to enlarge within the simulated granular matrix. Mounding could be reproduced, with the majority of the vertical displacement of the surface being attributable to reduction of the bulk density due to dilation of the granular matrix during root enlargement. Finally, we develop a previous analysis of the role of roots in transporting soil during growth and decay cycles. We find that even in shallow soils, the root-cycle can drive significant soil transport down forested montane slopes.

KEYWORDS: microtopography; biogeomorphology; tree root mounds; mobile regolith transport

Introduction

A major thrust of modern geomorphic research involves formulating process rules that can be incorporated in landscape evolution models (Dietrich *et al.*, 2003). Ideally, the process rule captures the dependence of the process on environmental factors that might change through time, including both climate and land-use. When investigating mobile regolith transport and the resulting evolution of hillslopes, the challenge is to identify the processes responsible for transport, and then to quantify how each process contributes to the movement of mobile regolith (hereafter simply called soil, because of the presence of roots). While significant progress has been made on physically-modulated processes responsible for the transport of soil, such as creep due to freeze–thaw (Matsuoka, 2001; Anderson, 2002) and wetting–drying cycles (Fleming and Johnson, 1975), few have addressed the roles of plants and animals in the landscape. Biogeomorphic processes, which arguably play the leading role in many landscapes (Viles, 1988; Schaetzl *et al.*, 1989; Butler, 1995; Gabet, 2000; Gabet *et al.*, 2003; Corenblit *et al.*, 2011), are a leading challenge for developing modern geomorphic theory.

Two biogeomorphic processes that contribute to soil transport involve the growth, death, and decay of vegetation (Gabet *et al.*, 2003; Wilkinson *et al.*, 2009). The first is tree throw: as trees are uprooted, some soil remains attached to the tree roots and is pulled out of the hillslope surface; this is called the root plate (Denny and Goodlett, 1956). As the fallen tree's roots decay, the sediment in the root plate is freed and falls back to the hillslope surface. This process results in a clear microtopographic signature: a pit remains where the tree roots were pulled from the ground, and a mound sits where the sediment in the root plate fell (Schaetzl and Follmer, 1990). Over long timescales, this tree throw process results in the mass downslope movement of sediment, which can be especially important on steep hillslopes (Schaetzl and Follmer, 1990; Scott *et al.*, 1995; Gabet *et al.*, 2003).

A second process, which has received comparatively little attention, is the *in situ* growth and decay of tree roots. As a large fraction (many tens of percent) of the volume of a plant is below ground, the roots could play an important role in stirring, moving, and propping the soil. As plant roots grow, they can exert radial pressure on the surrounding soil of up to approximately 900 kPa (Misra *et al.*, 1986; Bennie, 1991). This pressure can displace the surrounding soil, especially by deforming the ground surface. Years later, as these same roots decay, they form cavities in the soil that can be re-filled by sediment from above (Carson and Kirkby, 1972; Shubayeva and Karpachevskiy, 1983; Phillips and Marion, 2006).

Like tree throw, the process of root growth and decay results in a microtopographic signature on the hillslope surface. Small mounds of soil form around the bases of some tree trunks, pushed up above the surrounding topography by the pressures of the roots growing below (Richter *et al.*, 2007). Here, our first goal is to present the first detailed observations of the relationship between root volume, root size distribution, and the resulting microtopography.

Also like tree throw, root growth and decay causes mass downslope movement of soil (Carson and Kirkby, 1972). For a first-order approximation of this process, we assume that soil is incompressible. In this case, the volume of soil displaced normal to the hillslope by growth of a root should be equivalent to the volume of soil that subsides vertically to fill in the hole left upon decay of that root. The net effect is that a volume of soil is transported downslope by some distance that depends on the local slope. Hence, the process is diffusive. This root-growth-driven downslope movement of soil has not been treated in depth beyond its first mathematical formulation (Gabet *et al.*, 2003). A refinement of this mathematical treatment is a second goal of this paper.

While the likelihood that a given tree will die due to uprooting over depends on a variety of factors, including soil composition, local wind patterns, storm frequency, and the prevalence of pathogens (Schaetzl *et al.*, 1989), it is generally considered to be low. An estimate from one recent model involving a stand of Douglas Fir trees suggests that only 15% of trees die due to uprooting (Gabet and Mudd, 2010). However, all remaining trees, and all vegetation other than trees, will grow and die in one place. As their roots grow and decay, these plants will contribute to the mass transport of soil even though they are not being uprooted. Gabet *et al.* (2003) suggest that the downslope specific discharge of sediment due to tree throw is approximately four times greater than the specific discharge of sediment due to tree root growth and decay. This is undoubtedly dependent upon the species and the environmental setting that governs both the areal density of trees and the likelihood of tree uprooting. Root growth and decay will likely be of increased importance on hillslopes covered by vegetation other than trees, where tree throw cannot contribute to the mass downslope transport of sediment.

Field Sites and Root Mound Data

We documented the microtopography surrounding 23 Ponderosa Pine (*Pinus ponderosa*, subsp. scopulorum) and five Lodgepole Pine (*Pinus contorta*, subsp. latifolia) trees in two of the three sub-catchments within the Boulder Creek Critical Zone Observatory (BcCZO): Betasso and Gordon Gulch (Figure 1).

With mean elevations of 1934 m and 2627 m, these catchments lie within the foothills and montane geographic areas, respectively. The mean daily maximum and minimum temperatures at these sites are −7.3 °C (minimum, January) and 12.7 °C (maximum, July) at Betasso, and −9.2 °C (minimum, January) and 10.5 °C (maximum, July) at Gordon Gulch (Barry, 1973). The underlying bedrock consists of Precambrian crystalline rocks (granodiorites and high-grade metamorphic wall rocks into which they were intruded) that were exhumed during the Laramide Orogeny (~65 to 40 Ma; Dickinson *et al.*, 1988). In general, soils are poorly developed in this arid environment and range from loamy sands to sandy loams with minor (< 10%) clay and many subangular rock fragments. They are classified as Typic Happlustolls (see http://websoilsurvey.nrcs.usda.gov/app/WebSoilSurvey.aspx). Soil pits on site reveal that horizonation is weak. O horizons are thin (~ 5 cm), A horizons 5–20 cm, and weak B horizons are 30–40 cm thick. Underlying weathered rock in a Cox horizon grades into rock at around 80 cm (M. Foster, personal communication).

Tree species and tree density are strongly controlled by slope aspect in both catchments, south-facing slopes being dominated by Ponderosa Pine whereas north-facing slopes are dominated by Lodgepole Pine (see Figure 2). Modification by logging in the late 1800 s was apparently minor, and the tree cover had sufficient time to recover. As is commonly the case, the Ponderosa slopes are relatively open; trees are spaced tens to many tens of meters apart with intervening meadow grasses. Tree throw is relatively rare in these areas; hillslopes are generally smooth at short length-scales and are not marked by pits and mounds. Tree diameters can exceed 0.5 m. Lodgepole stands are much more dense; tree spacing is on the order of one to a few meters, and undergrowth is essentially absent. Tree diameters are more commonly less than 0.3 m.

We sampled Lodgepoles from north-facing slopes, and Ponderosas from south-facing slopes. Trees were chosen that were at least several meters away from any other trees, to assure that root mounds surrounding each tree would represent microtopography generated by that tree alone. We investigated only those trees that exhibited clear root mounding (Figures 3a and 3b), which represent ~75% of the trees in Betasso and Gordon Gulch catchments, based on a random sample of 100 trees. While it is clear, where observation is allowed by trail or road cuts, that tree roots also displace rocks in the saprolite

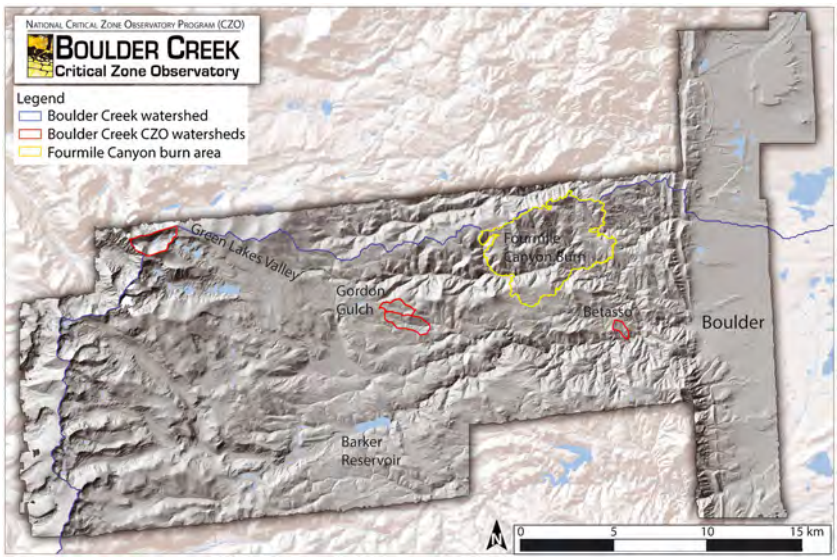

Figure 1. Boulder Creek watershed, Colorado. The Boulder Creek Critical Zone Observatory (BcCZO) comprises three subcatchments, the lower two of which, Gordon Gulch and Betasso, are forested and the targets of this study. Perimeter of Fourmile Canyon Fire area is also shown. This figure is available in colour online at wileyonlinelibrary.com/journal/esp

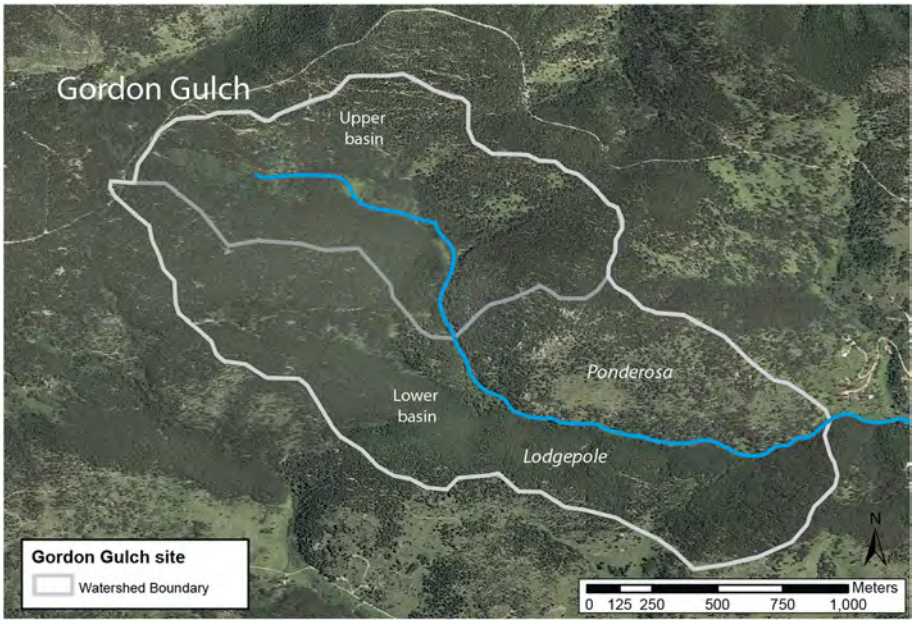

Figure 2. Air photograph of Gordon Gulch catchment in the BcCZO. Seen most clearly in lower basin, the south-facing slopes are open Ponderosa-dominated forest, and north-facing slopes are dense Lodgepole forest. This figure is available in colour online at wileyonlinelibrary.com/journal/esp

Figure 3. Root mounds surrounding two Ponderosa pines. (a) Global positioning system (GPS) for scale; (b) trenching tool for scale. Both fine sediment and coarse rocks can be seen in an annulus around each tree. While forest duff, dominated by pine needles, contributes to the topography, brushing away the pine needles reveals that the mound itself is dominantly soil. (c) Tree roots clearly penetrate rock subjacent to the soil in many places, inducing growth of existing fractures within the rock, and displacing both rock and overlying soil. Photographs by BSSH and RSA. This figure is available in colour online at wileyonlinelibrary.com/journal/esp

beneath the soil (Figure 3c), in general we are not able to discriminate between soil and saprolite displacements.

We measured the circumference of each tree at breast height, from which we calculated their diameter at breast height (DBH). Total tree volume and total below-ground volume can be calculated based on scaling relationships in the literature (e.g. Cockrell and Howard, 1968; Gibson *et al.*, 1986; McDonald and Skinner, 1989; Omdal *et al.*, 2001; Miles and Smith, 2009). For each tree, we measured the root mound at its base extending in four directions: upslope, downslope, to the left of the tree, and to the right of the tree (facing upslope, Figure 4). The distance from the soil surface (including top organic horizons) to a horizontal datum was taken at 10 cm increments, starting at the tree trunk and extending out 140 cm. We measured from the top organic horizons, which consisted of mainly pine needle litter, as we found that in the trees we sampled, the litter surrounding a given tree had uniform thickness out to at least 140 cm from the trunk. For all 28 trees we investigated, the clear root mound could not be detected at distances more than 140 cm away from the trunk.

The root mounds display a common profile shape. Figures 5–7 provide characteristic examples of the side-slope profiles, upslope profiles, and downslope profiles, respectively. Table I displays the basic data collected for each of the 23 Ponderosas and the five Lodgepoles studied. In all four directional profiles collected, root mound heights and widths were on the order of one to three decimeters. Cross-sectional areas under these profiles varied, but were all between 900 cm^2 and 3000 cm^2. In the case of side-slope

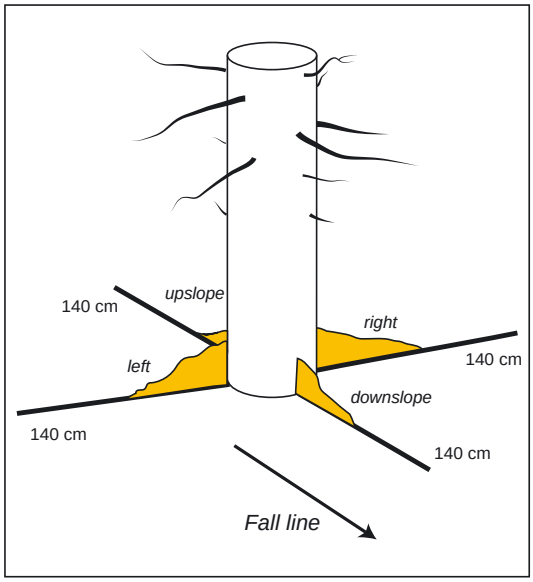

Figure 4. Sampling procedure. We documented tree circumference to calculate diameter at breast height (DBH), and topographic profiles in four directions, all measured with respect to a horizontal datum. This figure is available in colour online at wileyonlinelibrary.com/journal/esp

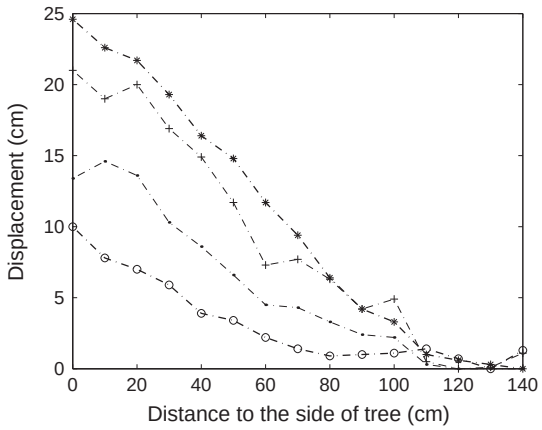

Figure 5. Some characteristic examples of side-slope topographic profiles. The root mound displacement relative to horizontal is greatest immediately adjacent to the tree trunk, reaching 10–25 cm. The mounds appear to be limited to distances within 80–130 cm from the trunk.

profiles, the average maximum vertical displacement was 12.2 cm, with standard deviation 6.1 cm. The average width was 93.3 cm (with standard deviation of 30.7 cm). The average cross-sectional area under the side slope profiles was 709 cm^2 (with standard deviation of 527 cm^2). The left- and right-slope profiles were commonly asymmetrical, which we address later. Both downslope and upslope profiles occasionally had negative cross-sectional areas when we attempted to separate the mound from the far-field slope, indicating a depression on that side of the tree rather than a mound.

One explanation for the mounding upslope of trees would be that the tree trunks are deflecting soil as it moves downslope. Soil can flow or creep downslope by a number of processes; in general, the transport rate is governed by the local slope of the surface, the thickness of the soil, and the intensity of the transport process (e.g. Anderson, 2002; Dietrich *et al.*, 2003). Conservation of mass requires that an obstacle in the path of such motion, in our case a tree trunk, should cause soil to accumulate upslope of the obstacle, and to thin downslope of it. In effect, the tree trunk generates a disturbance in the soil as if the tree were being forced uphill; a bow wave forms upslope of the

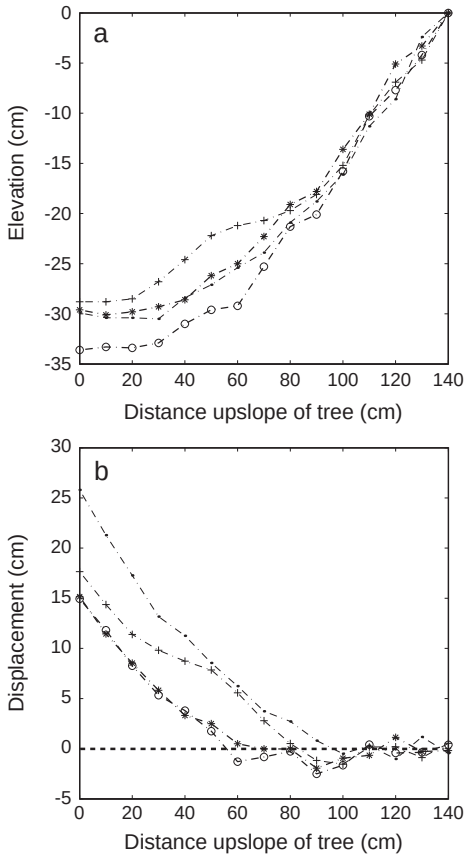

Figure 6. Some characteristic upslope profiles. (a) Unadjusted raw profiles relative to horizontal. The tree trunk is on the left. The slope of the hill declines as one approaches the tree trunk from upslope. (b) Vertical displacement profiles after adjustment by subtraction of the best-fitting far-field slope. Mounding near the tree trunk is more apparent; root mounds appear to extend 60–100 cm upslope from the trunk.

tree and a wake forms behind it. This evolution of the soil thickness should occur until the slope of the surface between the bow wave uphill and the wake downhill of the tree is sufficient to drive the diverging flow of material around the tree. At that point a steady surface profile will be established. In Figure 8 we show such a steady profile, achieved at the termination of a numerical simulation of soil creep on a two-dimensional (2D) surface with an embedded tree trunk of 0.3 m radius. We emphasize that in all calculations the deflection profile around the tree shows the same symmetry: upward deflection of the surface uphill of the tree, and downward deflection of the surface downhill of the tree. This is the opposite of what we observe around the Ponderosas we have studied. Figure 9 compares the cross-sectional area of the root mounds downslope of the sampled Ponderosas to the cross-sectional area of the mounds above the trees. If the upslope root mounds were due entirely to this deflection effect, then all the points would fall in the lower right-hand quadrant of Figure 9. This is not the case. In the majority of cases, the mounding is clear on both upslope and downslope sides of trees (shaded quadrant in Figure 9), We take this observation to imply that the rate of growth of a perturbation of the soil surface due to downhill flow of soil is trumped by the effect of the insertion of roots around the tree, at least in the landscapes we have studied.

In the case of the side-slope profiles, we were able to characterize 41 of the 46 Ponderosa profiles (left and right, for 23 trees) as being similar in shape to the profiles presented in Figure 3. For each of these profiles, we report the total vertical displacement relative to the local topography, and the width, measured outwards from the tree trunk, of the root mound. There was no

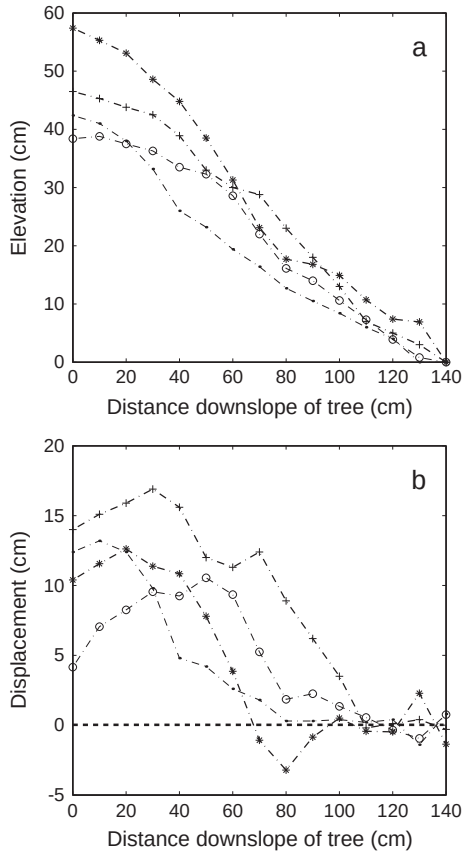

Figure 7. Some characteristic downslope profiles. (a) Unadjusted topographic profiles relative to horizontal. Downslope of the tree trunk, root mounds are less prominent. (b) Vertical displacement profiles after subtraction of the best-fitting far-field slope. The mounds appear to have amplitudes of about 10 cm, and are limited to 40–110 cm from the trunk.

correlation between the calculated below-ground root volume of the trees and both their associated root mounds' heights ($R^2 = 0.00054$ for linear regression) and widths ($R^2 = 0.00137$). There was also little correlation between the width (Figure 10a) and height (Figure 10b) of the mound on one side of the tree and its height and width on the other. Finally, for 17 of the 23 Ponderosas, we compared the sum of the cross-sectional area of the four profiles with the trees' diameter at breast height. There was no correlation ($R^2 = 0.05745$).

Discussion of Field Data

The lack of correlation between root mound sizes and calculated below-ground root volume is made more apparent when one considers one criterion used in selecting the trees for study, the implications of which we elaborate on in the end of this section: we selected only those trees with clear root mounds at their base. We found that ~25% of Ponderosas, of size comparable to those studied, did not display discernable root mounds at their bases. This lack of correlation between root volume and mound size is surprising, as is the lack of correlation between the sizes of root mounds on opposite sides of a tree. These observations deserve an explanation.

The differences in root mound sizes between trees of similar size may be due to local differences in the ongoing erosion of their root mounds. In their discussion of the evolution of the microtopographic mounds generated by tree-throw, Schaetzl and Follmer (1990) suggest that a number of factors may affect the erosion of microtopography; see also Ulanova (2000) and Samonil *et al*. (2010). Among them are: soil texture; soil permeability, porosity, and natural drainage; size and strength of soil aggregates; microclimate; coverage of litter on the mounds; faunal activity; surface wash and runoff processes. Each of these factors may have differed between any of the trees we sampled. For instance, some trees had large amounts of pine needle duff covering some or all of their root mounds, whereas some had very little. As the trees we sampled were taken from different points within the two drainages, they are likely exposed to different local hydrologic processes.

A second, more compelling, explanation augments this first one: the differences in root mound sizes between trees of similar size may be due to differences in the root architecture among the trees we sampled. Danjon *et al*. (2008) developed a three-dimensional (3D) model of the root architecture of two White Oaks (*Quercus alba*) near Athens, Georgia. The architecture of these two roots systems differed significantly: one tree has grown a taproot, the other has not. While pine trees were not studied, the study by Danjon *et al*. (2008) indicates that the root structure can vary greatly between two trees of the same species. This fact may explain some of the variation between root mound sizes in those trees studied that have similar calculated below-ground root volume. Variations in root architecture may also explain the variation in root mound size between the left and right sides of the sampled trees. In their 2008 paper, Danjon *et al*. (2008) note that several factors can cause radial asymmetry in the roots of a single tree: uneven distribution of water and nutrients around that tree, mechanical stresses induced by growth on a slope, and mechanical stresses due to dominant wind direction. Radial asymmetry in rooting patterns could cause asymmetries in both the height and width of the displaced root mounds.

Here we take advantage of an intense forest fire that occurred two years earlier on a nearby catchment – the Fourmile Canyon Fire of summer 2010 (Ebel *et al*., 2012). Many trees of the Ponderosa-dominated portion of this catchment were burned so completely that even roots burned. The fire burned along roots until it was smothered due to lack of oxygen. The result was small pits where the trunks used to be, with one to several lateral tunnels disappearing into the subsurface where roots burned (Figure 11). The pattern suggests that at least close to the tree trunk the angular distribution of root area will vary considerably from one tree to the next, reflecting the directions in which these major roots take off from the trunk.

Finally, we turn to the implications of our field data on the mass transport of soils on a hillslope. We found that three quarters of Ponderosas in the study area exhibited clear mounding caused by root growth. It follows that the roots of at least three quarters of Ponderosas contribute to the downslope movement of soil, as outlined in the Introduction. We expect that the remaining 25% of Ponderosa roots do contribute to soil movement in the same way. These trees insert their roots into the ground just like the other 75%, and these roots must displace soil around them. Possible explanations for the absence of mounds around these trees include those local variations in erosion already noted in this section. It is also possible that the root architecture of these trees leads to a more diffuse, subtler pattern of soil displacement that is difficult to differentiate from the local slope.

Discrete Element Method Simulations of Root Mounding

These observations inspire our attempt here to model the vertical displacement pattern around an isolated tree. We wish

Table I. Summary of data from tree root sites

Tree	DBH(cm)	L. Height (cm)	L. Width (cm)	L. Area (cm^2)	R. Height (cm)	R. Width (cm)	R Area (cm^2)	Up Height (cm)	Up Width (cm)	Up Area (cm^2)	Down Height (cm)	Down Width (cm)	Down Area (cm^2)
Ponderosa 1	28.3259	7.5	80	324	18.4	140	1540				8.1	110	555
Ponderosa 2	25.4615				23	140	1935	2.75	70	73.1	−11.4	50	−155.3
Ponderosa 3	27.0528	24.7	140	2079.5	18.5	100	263	0	0	0	17.8	100	1137.8
Ponderosa 4	41.3749	18.4	110	1468	5.9	80	390	0	0	0	−25.7	70	−810.8
Ponderosa 5	34.0547	19.2	140	1296.5	20	140	1839	0	0	0	10.6	80	587
Ponderosa 6	33.0999	12.9	120	974.5	10.2	110	668.5	2.7	90	212.7	7.2	100	315.65
Ponderosa 7	32.4634	7.7	120	418.5	18.7	120	1295.5	15	60	375.5	11.2	100	727.85
Ponderosa 8	59.198	9.7	110	678	23.6	110	1304.5	13.8	110	765	12.9	110	826.5
Ponderosa 9	44.8759	16.5	80	934.5	8.2	100	605.5	25.9	100	1221.5	16.9	110	1230.5
Ponderosa 10	21.0057	7.9	60	215.5	11.3	80	594	17.7	90	695.9	4.35	40	103.85
Ponderosa 11	22.5971	17	100	824.5	15	110	806	15.2	60	379.25	3.6	30	60
Ponderosa 12	32.7817	6.9	80	296	14.3	110	730	12.1	50	359.4	0	0	0
Ponderosa 13	21.9605	16.4	130	1163	22.7	120	1331	0	0	0	12.6	70	613.3
Ponderosa 14	32.9408				14.7	110	988.5	25.8	100	975.45	−10.8	100	−434.25
Ponderosa 15	42.648	7.2	60	302.5	11	80	597.5	53.5	140	2966.9	−9.75	60	−196.5
Ponderosa 16	56.3335							19.3	120	970.25	0	0	0
Ponderosa 17	26.4163	2.5	90	176.5				0	0	0	10.2	110	756.5
Ponderosa 18	29.9173	4	60	169	8.1	50	291						
Ponderosa 19	39.147	2.7	50	96	9.2	100	571	6.5	30	92.6	25.2	110	1520.5
Ponderosa 20	37.5557	20.5	110	1159.5	8.4	90	409.5	4.3	40	74.8	13.2	80	541
Ponderosa 21	38.1922	5.5	50	207	18	100	1068	20.1	90	816	0	0	0
Ponderosa 22	32.1451	2.4	50	81.5	10.9	80	549	−4.5	90	−219.7	13	80	569.85
Ponderosa 23	42.9663	6.2	50	131	21.3	140	1642	0	0	0	−12.6	60	−356.25
Lodgepole 1	21.0057	12.4	120	606	8.5	30	132.5	23.75	70	738	27.4	100	1876.1
Lodgepole 2	25.4615	7.7	70	309.5	10.6	50	337	14.2	60	357.25	13.4	110	819.5
Lodgepole 3	22.2788	18.6	120	919.5	9.2	70	335	0	0	0	−22.1	100	−896.75
Lodgepole 4	23.5519	5.4	70	158	6.9	60	122	11.1	20	84.4	15.2	110	846.5
Lodgepole 5	21.9605	10	130	639	7.8	40	169	0	0	0	10.7	90	703.7

Note: Blanks indicate cases where the profiles could not be characterized as similar to the examples given in Figures 5–7. Upslope and downslope data are reported after subtraction of far-field slope, as in Figures 6b and 7b.

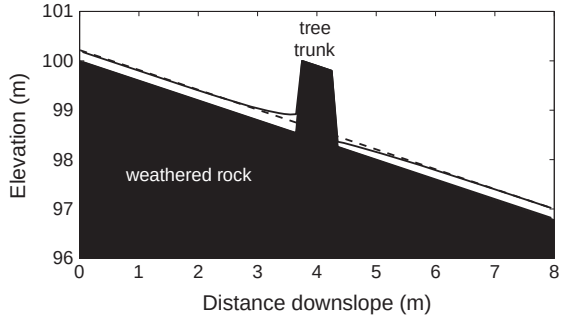

Figure 8. Simulated hillslope profile around a tree trunk, due entirely to deflection effects. Note the upward deflection of the surface uphill of the tree, and the downward deflection of the surface downhill of the tree. The downhill profile is the opposite of what we observed.

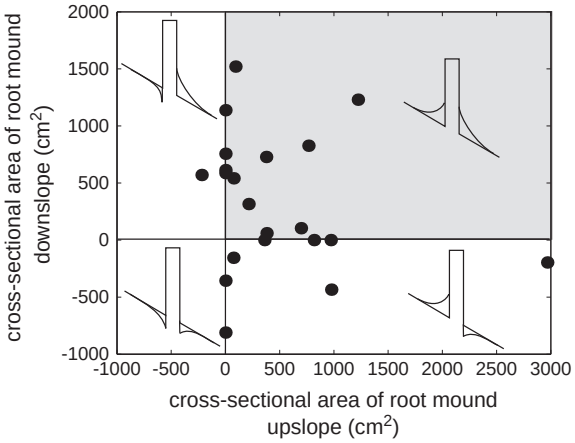

Figure 9. Comparison of the cross-sectional area of the downslope and upslope profiles, after subtraction of far-field slope. Light lines separate quadrants of mounding behavior as indicated in sketches. The lower right quadrant reflects the profile we would expect if the local slope was governed entirely by the deflection of creeping soil around the trunk, as in the previous figure. The gray shaded quadrant, in which most data lie, indicates mounding is positive on both upslope and downslope sides of the tree, implicating root-induced displacement.

to explore the degree to which the mound shape and magnitude surrounding a tree can be captured in a simulation in which a set of roots with a specified distribution is inserted into a granular soil. While a number of root growth models exist, with styles that range from discrete architectural models to continuous models (see Dupuy *et al.*, 2010, for a review), we have opted to employ a model in which deformation of the granular medium is explicitly taken into account. It is after all the deformation of the soil matrix with which we are concerned here. Discrete element method (DEM) simulations, first developed by Cundall and Strack (1979), have been used to study various geomorphically relevant granular phenomena, from aeolian saltation (Haff and Anderson, 1993) to large-scale granular flows (Walton, 1993; Silbert *et al.*, 2001). We used the open-source DEM LIGGGHTS (liggghts.com, 2012; see Vedachalam (2011) and Chand *et al*. (2012) for recent applications), an expansion of the molecular dynamics simulator LAMMPS designed for improved granular simulations. We simulated in two dimensions the growth of roots below a tree and the resulting mounding of soil.

Particles were modeled as small spheres constrained to move in two-dimensions. Particle contacts were modeled as Hertzian springs (linear elastic mechanics in which contact forces go as indentation depths), ignoring rolling friction (for technical details of the LIGGGHTS code and its options, see Antypov and Elliott (2011) and Chand *et al*. (2012) for an in-depth

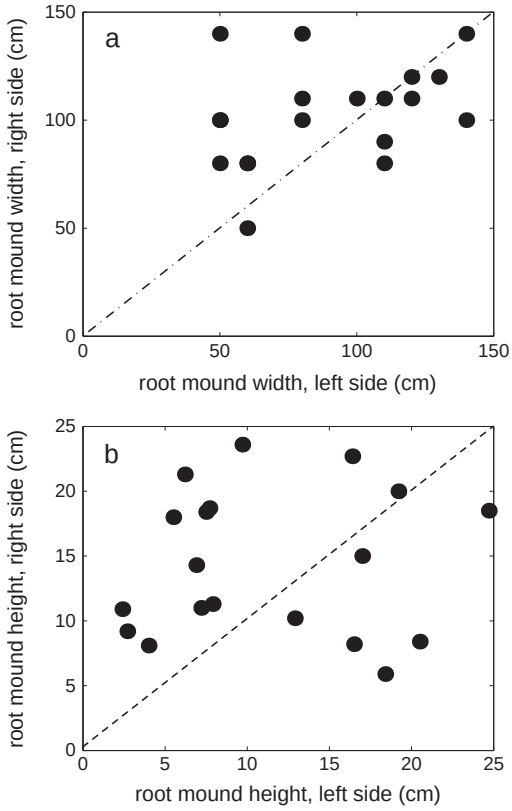

Figure 10. Testing the symmetry of root mounds. (a) Comparison of root mound widths on the left and right sides of sampled trees. (b) Comparison of measured root mound heights on the left and right side of sampled trees. Perfect symmetry would be implied if all data fell on 1:1 line. Strong scatter implies mounding is significantly asymmetrical. Note that there is little correlation between the two, meaning that the mounds are commonly asymmetric in this cross-slope dimension.

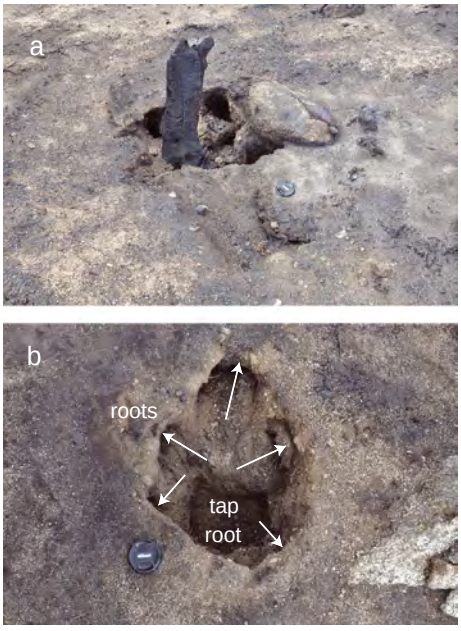

Figure 11. Photographs of burned tree sites within the Fourmile Fire area, Fourmile Canyon, Colorado. (a) Small remnant of tree trunk remains unburned, while several roots have burned to well below-ground level. (b) Tree and major roots are entirely removed by fire. Tap root and several major lateral roots leave holes as the roots burned to well below-ground surface. Camera lens cap for scale in both photographs. Photographs by RSA. This figure is available in colour online at wileyonlinelibrary.com/journal/esp

discussion). Relevant simulation parameters are given in Table II. For efficiency of calculation, the simulation was run at 1/100th length scale (Figure 12). Changing the length scale did not change our simulation results, which depended instead on the geometry of the simulated particles. A Young's modulus for the soil particles was chosen to be 1 GPa, rather than the typical value of 10 GPa for real rocks. A more realistic value of Young's modulus would require a much shorter time step to avoid unrealistic particle indentations, and accelerations, and thus would be much more computationally expensive. At the chosen value, particles (both soil particles and tree root particles) are still sufficiently stiff to capture the rigid behavior in the natural system, and the results of our calculations were insensitive to this specific choice. Other material properties resembled measured values for quartz. The simulation was run in two phases. In the first phase, 2.2×10^5 monodisperse soil particles were randomly poured into a 30 m long, 15 m tall box (real-world scales, i.e. after 1:100 scaling noted earlier) with a smooth wall on the floor and periodic boundary conditions in the x-direction. Once the soil settled, all particles above 7.5 m were deleted.

In the second phase, a cylindrical lattice of closely spaced soil-type particles was added above the soil surface to represent the tree trunk, and these particles were fixed in place. Root particles were inserted in a grid, with 70 cm between orthogonal roots, in a cone-shaped region centered beneath the tree trunk (see Figure 12). As a first approximation of root cone dimensions, we use averages of Ponderosa Pine root cone dimensions reported by Stone and Kalisz (1991). Both broad and narrow root cones were used, in order to reflect some of the variability that Stone and Kalisz (1991) report naturally occurs in root cone dimensions. We acknowledge that many other distributions could be chosen, and that appropriate distributions will differ among tree species. The gravity vector was chosen to simulate both flat surfaces and angled slopes. The roots grew to a final size, displacing the soil particles above them in a mound around the tree trunk. Figure 13 displays the root mound profiles for the two different root cone shapes simulated on flat ground (slope angle 0°).

The profiles in Figure 13 are comparable in shape to the measured vertical displacement profiles shown in Figure 5. The scale of the mound width is much larger in the simulation than those observed in the field. In the simulations, root mound widths were comparable to the imposed pattern of roots, which is governed by the cone widths. The difference between measured and simulated mound widths could therefore be due to a difference in rooting patterns of the trees reported by Stone and Kalisz (1991) – which we used to set root cone dimensions in our simulations – and those of the trees whose root mounds we measured in the field. Alternatively, the difference could result from denser, more compressed soils around real trees. Or finally, this difference could be due to natural limits on the field measurement of the mounds. While mounding may have been present at distances of 5 or 10 m from the tree trunk in the field, the vertical amplitude of the displacement at these distances was too small to be differentiated from local noise in the topographic profile.

One striking feature of the profiles in Figure 13 is the variation between the left and right mounds for the broad root distribution, which was symmetrical about the tree axis. Given the symmetrical set-up for this simulation, we can only attribute this to local variations in soil structure, meaning here the detailed packing of the soil particles. This effect likely contributes to the asymmetries in left and right profiles seen in the field examples depicted in Figure 10. A second feature of the profiles in Figure 13 is that, for both broad and narrow root distributions, the width of the mound profile reflected the

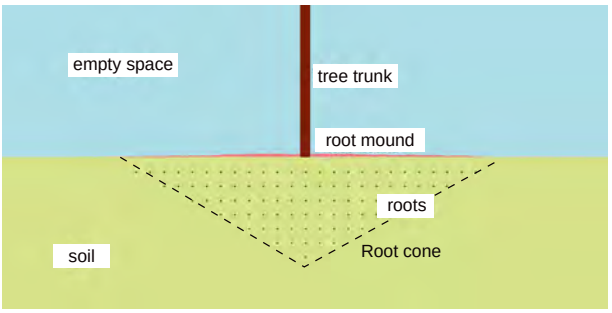

Figure 12. Simulation set-up, for root cone of radius 10 m, depth 5 m (after adjusting for scale). Box dimensions are 30 m by 15 m. Soil is composed of disks with diameter 0.035 m. All roots begin with diameter 0.035 m, and grow to diameters of 0.1 m, displacing surface of soil into a mound around the tree trunk (pink) above the initial soil surface (green). This figure is available in colour online at wileyonlinelibrary.com/journal/esp

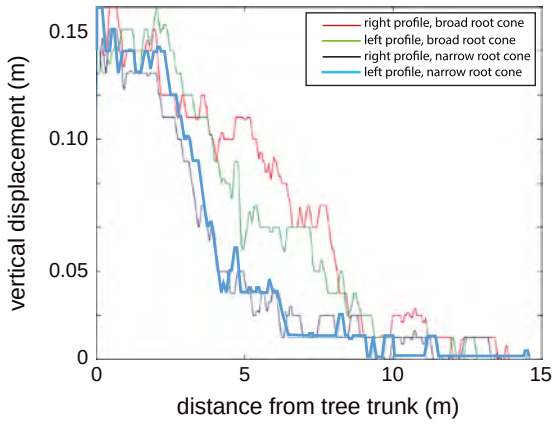

Figure 13. Root mound profiles for the two simulations for a flat surface. Simulations differ only in that the cone-shaped pattern within which roots are placed differs in its cone angle. This figure is available in colour online at wileyonlinelibrary.com/journal/esp

Table II. Parameters for LIGGGHTS simulations

Particle density (kg/m^3)	2500	Diameter of soil particles (m)	0.035
Young's Modulus (GPa)	1.0	Starting/ending root diameter (m)	.035/0.1
Poisson Ratio	0.25	Tree trunk diameter (m)	0.5
Restitution coefficient	0.7	Time steps (phase 2)	500000
Grain–grain, grain–wall friction coefficient	0.5	Time step size (phase 2)	5×10^{-9}
Root cone radius (m)	10, 5	Root cone depth (m)	5, 7
Slope angle (deg)	0, 15, 30	Number of roots	91, 66

Note: Density, Young's modulus, Poisson ratio, coefficient of restitution, and coefficient of friction are for both soil and root particle types. Root cones took two shapes – broad and narrow – constrained by the maximum axial and radial root extents for Ponderosas given in Stone and Kalisz (1991).

width of the root distribution. This confirms that root distribution also plays a significant role in determining root mound shape, as argued in the previous section.

Also noteworthy was the cross-sectional area of the simulated root mounds. In the case of the broad root distribution, the 91 roots added to the system produced a total root cross-sectional area of 0.72 m^2, while the root mound produced had a cross-sectional area of 1.78 m^2, about 2.5 times greater. And in the narrow case, the 66 roots with 0.52 m^2 of root area produced a mound with 1.20 m^2, about 2.3 times greater.

Comparison of the mounding simulated on different slopes (Figure 14) suggests that mounding occurs in much the same way on a steep slope (30°) as on a flat one. If this is correct, the asymmetrical shapes of the upslope and downslope profiles seen in Figures 6 and 7, and discussed in the previous section, would then be attributable not to asymmetries of root displacement patterns on a slope, but to differences in erosion or rooting patterns, as discussed earlier, or to the contributions of long-term root decay beneath a tree. Alternatively, asymmetries of root displacement patterns on a slope may occur naturally and our model may be imperfect.

Root-mounding as a Soil Transport Process

Finally, we revisit and develop some earlier work on the role of root cycling as a soil transport process. Such a calculation must honor the role of growth and decay of individual roots on individual trees (a root event), the depth-distribution of such events, and the frequency of such events. Gabet *et al.* (2003) developed the first analytic model of the effects of root mounding on soil transport. In this section, we provide some theoretical refinements to this model, and compare the importance of root mounding to soil transport in the three ecosystems studied within the BcCZO.

Gabet *et al.* (2003) treat the problem as follows. They seek the total downslope specific discharge q (in m^2 yr^{-1}) of soil due to root mounding, given a hillslope of angle θ with respect to the horizontal plane (Figure 15). As they assume that the soil is incompressible, the soil displaced by the root normal to the hillslope surface will have the same volume as the root. The net downslope movement of this soil, X (in meters, see Figure 15), is then given by $X = z\sin\theta$, where z is the vertical depth to the root center (in meters). The factor $\sin(\theta)$ reflects the fact that the soil falls vertically, while it is assumed to be displaced normal to the slope during root growth. We must then assume something about the distribution of roots with depth. The cumulative probability of root distribution may be cast as:

$$Y = 1 - \beta^{100z} \tag{1}$$

where $0 < \beta < 1$ is a dimensionless parameter that depends on tree species, and Y is the cumulative root fraction with depth, the integral of the probability density function of roots with depth (Figure 16b). In Equation 1, β is taken to the power of $100z$ rather than simply z because we are converting between centimeters and meters, since the parameter β was developed for use with centimeters in Gale and Grigal (1987). The value

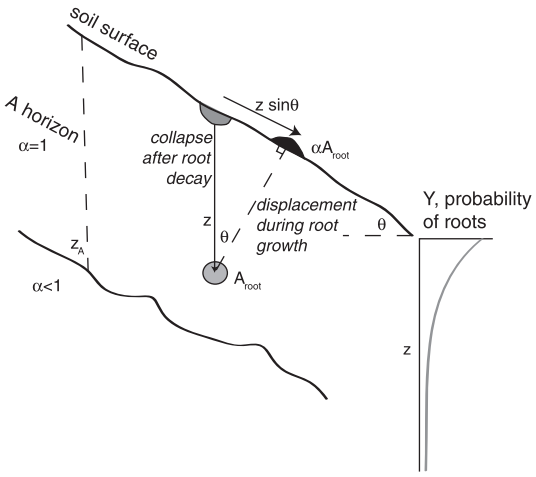

Figure 15. Setup of the problem of soil transport by root growth and decay, modified from Gabet *et al.* (2003). Root growth and decay cycle is shown for a root of cross-sectional area, A. A fraction of that area, denoted α, results in surface displacement, the remainder contributing to compaction of the local soil surrounding the root. The cycle results in displacement of soil normal to the surface during growth (black) and collapse of soil during decay (gray). Right: sketch of probability density of root depths, $Y(z)$.

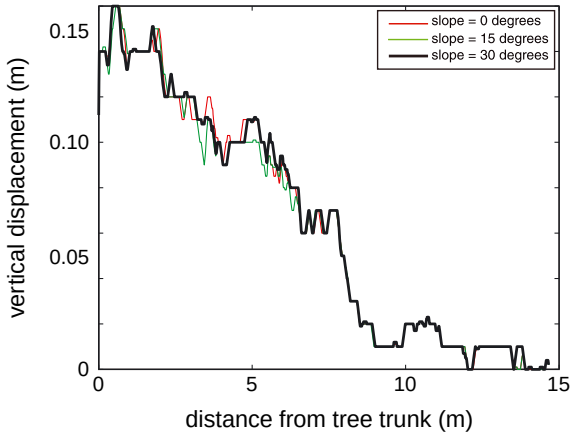

Figure 14. Right root mound profiles, broad root distribution, for three different slopes. Variation of slope angle from 0° to 30° did not affect root mound shape significantly. This figure is available in colour online at wileyonlinelibrary.com/journal/esp

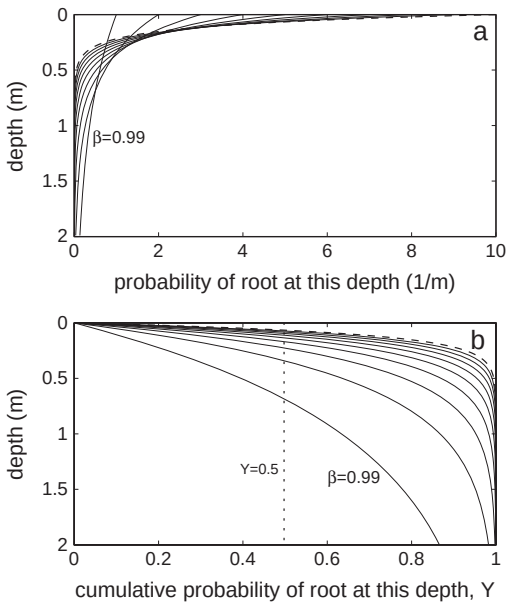

Figure 16. Rooting depth distributions. (a) Probability distributions of rooting depths for various distribution parameters, β. Plotted are cases with $\beta = 0.99$ (labeled) through $\beta = 0.90$ (dashed). (b) Cumulative root distributions, Y as a function of depth (Equation 1). Intersection of these curves with $Y = 0.5$ (dotted) indicates depth to mean rooting depth.

of β typically lies between 0.90 and 0.98, where larger values correspond to deeper rooting profiles (Gill and Jackson, 2000). Equation 1 is the integral form of the probability density of roots with depth (Figure 16a):

$$y = 100\beta^{100z}\log\beta \tag{2}$$

Following Gale and Grigal (1987), we may solve Equation 1 for rooting depth by:

$$z = \frac{\log(1-Y)}{100\log\beta} \tag{3}$$

To calculate downslope soil specific discharge, q, Gabet *et al.* (2003) multiply X by total root mass per unit area, r (in kg m^{-2}), and the annual root turnover frequency τ (in yr^{-1}) (which varies from zero to one; see Gill and Jackson (2000)), and divide by the mass density of the root material, ρ_r (in kg m^{-3}). Setting Y to 0.5 to represent the average rooting depth, this yields:

$$q = -\frac{0.003r\tau}{\rho_r\log\beta}\sin\theta \tag{4}$$

In effect, this procedure assumes that all roots occur at the mean rooting depth, where $Y = 0.5$. We seek to relax this assumption, and to acknowledge the possibility that the efficiency of conversion of root cross-section to vertical displacement depends upon the depth of the root. Richter *et al.* (2007) argue based on a comparison of soil bulk densities that the pressure exerted on the surrounding soil by growing roots is relieved in different ways, depending on the soil horizon in which the root is growing. In the A horizon, they found that the soil surrounding roots had a bulk density (1.2–1.4 g cm^{-3}) comparable to that of soil at distances of 50 to 100 cm from tree roots. In the B horizon, they found that the soil surrounding roots had a bulk density (1.7–1.9 g cm^{-3}) greater than that of soil at distances of 50 to 100 cm from tree roots (1.5–1.7 g cm^{-3}). In the C horizon, they found a more subtle density difference (1.4–1.5 g cm^{-3} compared to 1.3–1.4 g cm^{-3}). The authors conclude that all root growth pressures in the A horizon are relieved by upward displacement of soil, whereas all root growth pressures in the B and C horizons are relieved by soil compaction. So, according to Richter *et al.*'s (2007) results, depending on the root profile and the depth of the A horizon on a hillslope, Gabet *et al.*'s (2003) assumption that all roots are located at the average rooting depth $Y = 0.5$ may or may not lead to a correct prediction of downslope soil specific discharge.

While it is likely that root growth pressures are relieved in different ways depending on the location of the roots in the soil, Richter *et al.*'s (2007) conclusion may also be too simplistic. In addition to the composition of the surrounding soil – which is reflected by its horizon – the depth at which a root grows likely determines how the surrounding soil relieves pressure. It is also likely that the boundary between the section of soil that relieves pressure entirely by upward displacement, and the section of soil that relieves pressure entirely by compression is more fuzzy than the horizon-based analysis would suggest. Richter *et al.*'s (2007) research therefore represents an approximation of how root growth pressures are relieved, one that we employ in our calculations and discussion. We suggest, however, that this is an area for potential further research, one that would improve upon our analysis of the geomorphic effects of root growth and decay. To accommodate the potential role of root location, we therefore make the following revisions to Gabet *et al.*'s (2003) analysis.

Considering again the setup of the problem employed by Gabet *et al.* (2003),the cumulative root volume per unit hillslope surface area, V (in m^3 m^{-2}) is given by:

$$V = \frac{r}{\rho_r}\left[1-\beta^{100z}\right] \tag{5}$$

Using Richter *et al.*'s (2007) result, we will eventually consider only roots in the A horizon. We may then assume that soil is incompressible, so that the volume of soil displaced by a root will be equal to the volume of the root. Taking the derivative of V with respect to depth, z, yields displaced soil volume per unit hillslope area per unit depth, as a function of depth:

$$\frac{dV}{dz} = -100\frac{r}{\rho_r}\ln\beta\left(\beta^{100z}\right) \tag{6}$$

We multiply by $X = z\sin\theta$, the distance downslope that the displaced sediment effectively moves as a function of depth, and by τ (in yr^{-1}), the root turnover rate, to find the downslope soil volume specific discharge, q, per unit depth, as a function of depth:

$$\frac{dq}{dz} = -100\frac{\tau r}{\rho_r}\ln\beta\left(z\beta^{100z}\right)\sin\theta \tag{7}$$

We now incorporate Richter *et al.*'s (2007) result. Since only the roots growing in the A horizon contribute to downslope movement of soil, we integrate from $z = 0$ to z_A to find q, where z_A is the depth of the lower A-horizon boundary, measured vertically from the soil surface. Hence,

$$q = -100\frac{\tau r}{\rho_r}\ln\beta\left[\int_0^{z_A} z\beta^{100z}dz\right]\sin\theta \tag{8}$$

Integrating by parts yields:

$$q = \frac{\tau r}{\rho_r}\left[\frac{\beta^{100z_A}-1}{100\ln\beta} - z_A\beta^{100z_A}\right]\sin\theta \tag{9}$$

We suspect that this formulation will yield a lower limit on the transport efficiency of this root mounding process, as root growth from depths greater than z_A may accomplish at least some vertical motion of the soil; i.e. $\alpha > 0$. In the event that

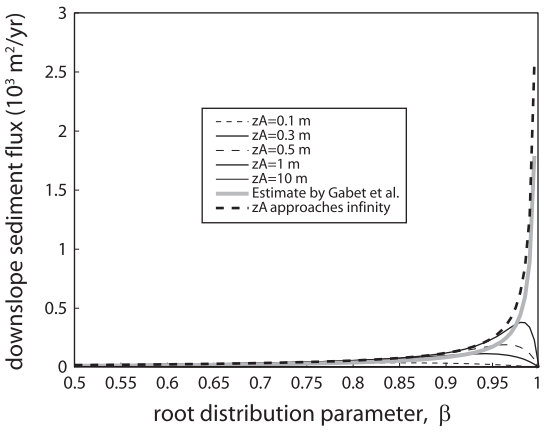

Figure 17. Comparison of specific discharge estimates for different values of N and z_A. The case plotted is for a 15° slope, with $\tau = 0.45$ yr^{-1}, $r = 4.4$ kg m^{-2}, and $\rho_r = 400$ kg m^{-3}, as in the temperate forests summarized in Table III.

Table III. Calculations of downslope volumetric specific discharge for the two forested Boulder Creek Critical Zone Observatory (BcCZO) study sites

CZO Site	Ecosystem	MAT (°C)	τ (yr^{-1})	r ($kg\,m^{-2}$)	ρ_r ($kg\,m^{-3}$)	β	z_A (m)	q ($m^2\,yr^{-1}$), Equation 2	q ($m^2\,yr^{-1}$), Gabet *et al.* (2003)
Betasso/GG	Temperate forest	10	0.45	4.4	400	0.98	0.15	$1.07\times10^{-4}\sin\theta$	$1.43\times10^{-3}\sin\theta$

Note: Mean annual temperature (MAT) for both sites and z_A for Betasso were taken from BcCZO website (http://czo.colorado.edu/, 2012), τ is based on MAT and Gill and Jackson (2000), r and β are due to Jackson *et al.* (1996), ρ_r is an estimate based on Gibson *et al.* (1986).

all root growth results in mounding, as in Gabet *et al.*'s (2003) calculation, we simply let z_A approach infinity. Since $0<\beta<1$, in this case

$$q = -\frac{r\tau}{\rho_r 100 \ln\beta}\sin\theta \tag{10}$$

This is about 40% larger than Gabet *et al.*'s (2003) calculated specific discharge (Equation 2), reflecting the difference between the integration of the full root distribution versus assuming that all roots occur at the mean distance from the surface.

In Figure 17 we compare the specific discharge predicted by Gabet *et al.* (2003) with the specific discharge predicted by Equation 9, for different values of β and A-horizon thickness, z_A. When the A-horizon is fixed at some finite depth, q increases to a maximum for some β, and then decreases towards zero as β approaches one. For thin A-horizons, the downslope specific discharge is small, and the maximum occurs at values of β that represent shallow root distributions. For example, if $z_A = 0.1$ m, the soil specific discharge q is always less than $4\times10^{-5}\,m^2\,yr^{-1}$, and reaches a maximum near $\beta = 0.8$. As the A-horizon thickens, q reaches its maximum at values of β that are increasingly closer to one, and this maximum becomes larger and more pronounced. For instance, if $z_A = 1$ m, q increases from less than $6\times10^{-5}\,m^2\,yr^{-1}$ at $\beta = 0.8$, to about $3.8\times10^{-4}\,m^2\,yr^{-1}$ at $\beta = 0.98$. In the ideal case all root growth occurs within a thick A-horizon, and hence contributes to soil mounding, the specific discharge of soil increases monotonically, approaching infinity as β approaches one, as in Gabet *et al.*'s (2003) estimate.

Using Equation 2, we calculate downslope specific discharge for the temperate forest ecosystems represented by the Betasso and Gordon Gulch sites studied within the BcCZO (Table III). In doing so, we assume that 100% of trees contribute to this process. As discussed previously, it is possible that as little as 75% of trees do so, although we suspect this is not the case. We see that, given the shallow A horizons in the areas studied within the BcCZO, the calculated downslope specific discharge of soil is a factor of 10 smaller than that predicted by the model of Gabet *et al.*'s (2003).

Finally, we return to the assumption of horizon-dependent response to root growth. In the weakly developed soils of the montane Front Range, horizons only weakly developed. We expect that in such settings, the response of the soil to root growth will not obey precisely these horizons, but will depend upon depth into the soil in some complex way that should serve as a target for further research. While the analysis we have presented is horizon-based, it nonetheless acknowledges the reality of a depth distribution of roots. The approach can easily be modified to acknowledge any depth dependence of the response of soil to root growth.

Conclusions

The growth of roots significantly inflates the soil surrounding the majority of Ponderosa pines in the BcCZO montane forests. In our data set, the volume of the mounds is only poorly related to the diameter of the trees. The upward displacement of soil on both upslope and downslope sides of trees implicates the growth of roots in the subsurface as the mounding mechanism, rather than the deflection of creeping soil as it encounters a tree trunk. Asymmetry of cross-slope profiles of mounds surrounding individual trees likely reflects the details of the root architecture, in which the locations of major roots likely play a significant role.

Using a numerical discrete element code, we produce mounding of the granular medium in which simulated root nodes were allowed to expand. Significant mounds were generated with cross-sectional shapes that mimicked those observed in the field. A large fraction of the vertical displacement reflects the dilation of the overlying soil during insertion of roots. Mound profiles can differ depending on the configuration of the soil matrix, and are not strongly dependent upon slope angle.

Root growth and decay cycles can lead to significant net displacement of soil. Following earlier work (Gabet *et al.*, 2003), the transport is linearly related to the local slope and is hence diffusive. The effective diffusivity is tied to the root turnover timescale, and the total root mass in the subsurface. We further explored the role of the vertical distribution of roots, and quantified the reduction in soil discharge to be expected when roots grow in soil horizons where isotropic densification of the soil rather than vertical displacements accommodates root growth.

We have presented data and a mechanism showing that trees can contribute significantly to downhill soil movement even if they are not uprooted. Climatic and land-use driven changes in the forest cover on a landscape could potentially strongly affect the soil discharge from hillslopes.

Acknowledgements—The authors thank David Dethier for field assistance and discussion during one of the field excursions, and Scott McCoy for his assistance in launching the discrete element modeling efforts using the LIGGGHTS code. The authors also thank Andy Wickert for detailed comments on an earlier version of the manuscript, Melissa Foster for soils descriptions at the sites, and both E. Gabet and an anonymous reviewer for very thorough and helpful comments on this manuscript. This research was funded by the National Science Foundation grant EAR-0724960 (the Boulder Creek Critical Zone Observatory).

References

Anderson RS. 2002. Modeling of tor-dotted crests, bedrock edges and parabolic profiles of the high alpine surfaces of the Wind River Range, Wyoming. *Geomorphology* **46**: 35–58.

Antypov D, Elliott J. 2011. On an analytical solution for the damped hertzian spring. *EPL* **94**(50004). DOI. 1209/0295-5075/94/5004

Barry RG. 1973. A climatological transect on the east slope of the Front Range, Colorado. *Arctic and Alpine Research* **5**: 89–110.

Bennie A. 1991. Growth and mechanical impedance, In *Plant Roots: The Hidden Half*. Marcek Dekker: New York; 393–414.

Butler D. 1995. *Zoogeomorphology*. Cambridge University Press: Cambridge.

Carson MA, Kirkby MJ. 1972. *Hillslope Form and Process*. Cambridge University Press: Cambridge.

Chand R, Khaskheli M, Qadir A, Ge B, Shi Q. 2012. Discrete particle simulation of radial segregation in horizontally rotating drum: effects

of drum-length and non-rotating end-plates. *Physica A: Statistical Mechanics and its Applications* **391**: 4590–4596

Cockrell RA, Howard RA. 1968. Specific gravity and shrinkage of open grown ponderosa pine. *Wood Science and Technology* **2**: 292–298.

Corenblit D, Baas A, Bornette G, Darrozes J, Delmotte S, Francis R, Gurnell A, Julien F, Naiman R, Steiger J. 2011. Feedbacks between geomorphology and biota controlling earth surface processes and landforms: a review of foundation concepts and current understandings. *Earth-Science Reviews* **106**: 307–331.

Cundall P, Strack O. 1979. A discrete numerical model for granular assemblies. *Geotechnique* **29**(1): 47–65.

Danjon F, Barker D, Drexhage M, Stokes A. 2008. Using three-dimensional plant root architecture in models of shallow-slope stability. *Annals of Botany* **101**: 1281–1293.

Denny C, Goodlett J. 1956. Microrelief Resulting from Fallen Trees. Surficial Geology and Geomorphology of Potter County, Pennsylvania. US Geological Survey Professional Paper 288. US geological Survey: Reston, VA; 59–66.

Dickinson W, Klute M, Hayes M, Janecke S, Lundin E, McKittrick M, Olivares M. 1988. Paleogeographic and paleotectonic setting of Laramide sedimentary basins in the central Rocky Mountain region. *Geological Society of America Bulletin* **100**(7): 1023.

Dietrich W, Bellugi D, Sklar L, Stock J, Heimsath A, Roering J. 2003. *Geomorphic Transport Laws for Predicting Landscape*, AGU Geophysical Monograph 135. American Geophysical Union: Washington, DC; 1–30.

Dupuy L, Gregory PJ, Bengough AG. 2010. Root growth models: towards a new generation of continuous approaches. *Journal of Experimental Biology* **61**(8): 2131–2143.

Ebel BA, Moody JA, Martin DA. 2012. Hydrologic conditions controlling runoff generation immediately after wildfire. *Water Resources Research* **48**: W03529. DOI. 10.1029/2011WR011470

Fleming R, Johnson A. 1975. Rates of seasonal creep of silty clay soil. *Quarterly Journal of Engineering Geology* **8**: 1–29.

Gabet EJ. 2000. Gopher bioturbation: field evidence for nonlinear hillslope diffusion. *Earth Surface Processes and Landforms* **25**(13): 1419–1428.

Gabet EJ, Mudd SM. 2010. Bedrock erosion by root fracture and tree throw: a coupled biogeomorphic model to explore the humped soil production function and the persistence of hillslope soils. *Journal of Geophysical Research* **115**: F04005. DOI. 10.1029/2009JF001526

Gabet EJ, Reichman O, Seabloom EW. 2003. The effects of bioturbation on soil processes and sediment transport. *Annual Reviews of Earth and Planetary Science* **31**: 249–273.

Gale M, Grigal D. 1987. Vertical root distributions of northern tree species in relation to successional status. *Canadian Journal of Forestry Research* **17**: 829–834.

Gibson M, McMillin C, Shoulders E. 1986. Moisture content and specific gravity of the four major southern pines under the same age and site conditions. *Wood and Fiber Science* **18**(3): 428–435.

Gill R, Jackson R. 2000. Global patterns of root turnover for terrestrial ecosystems. *New Phytology* **147**: 13–31.

Haff PK, Anderson RS. 1993. Grain scale simulations of loose sedimentary beds: the example of grain-bed impacts in aeolian saltation. *Sedimentology* **40**: 175–198.

Jackson R, Canadell J, Ehleringer J, Mooney H, Sala O, Schulze E. 1996. A global analysis of root distributions for terrestrial biomes. *Oecologia* **108**: 389–411.

Matsuoka N. 2001. Solifluction rates, processes and landforms: a global review. *Earth-Science Reviews* **55**: 107–134.

McDonald P, Skinner C. 1989. *Local Volume Tables for Young-growth Conifers on a High Quality Site in the Northern Sierra Nevada*, USDA Forest Service Research Note PSW-404. USDA: Washington, DC.

Miles P, Smith WB. 2009. *Specific Gravity and Other Properties of Wood and Bark for 156 Tree Species found in North America*, USDA Forest Service Research Note NRS-38. USDA: Washington, DC.

Misra RK, Dexter AR, Alston AM. 1986. Maximum axial and radial growth pressures of plant roots. *Plant and Soil* **95**: 315–326.

Omdal DW, Jacobi WR, Shaw CG III. 2001. Estimating large-root biomass from breast-height diameters for ponderosa pine in northern New Mexico. *Western Journal of Applied Forestry* **16**: 18–21.

Phillips JD, Marion DA. 2006. Biomechanical effects of trees on soil and regolith: beyond treethrow. *Annals of the Association of American Geographers* **96**: 233–247.

Richter DD, Oh NH, Fimmen R, Jackson J. 2007. The Rhizosphere and soil formation. In *The Rhizosphere*. Elsevier: Amsterdam; 179–200.

Samonil P, Král K, Hort L. 2010. The role of tree uprooting in soil formation: a critical literature review. *Geoderma* **157**: 65–79.

Schaetzl RJ, Follmer LR. 1990. Longevity of treethrow microtopography: implications for mass wasting. *Geomorphology* **3**: 113–123.

Schaetzl RJ, Johnson DL, Burns SF, Small TW. 1989. Tree uprooting: review of terminology, process, and environmental implications. *Canadian Journal of Forestry Research* **19**: 1–11.

Scott AN, Randall J, Schaetzl TWS. 1995. Effects of slope angle on mass movement by tree uprooting. *Geomorphology* **14**: 19–27.

Shubayeva VI, Karpachevskiy LO. 1983. Soil–windfall complexes and pedogenesis in the Siberian Stone Pine forests of the maritime territory. *Pochvovedeniye* **9**: 96–103.

Silbert L, Ertas D, Grest G, Halsey T, Levine D, Plimpton S. 2001. Granular flow down an inclined plane: Bagnold scaling and rheology. *Physical Review E* **64**(051302).

Stone E, Kalisz P. 1991. On the maximum extent of tree roots. *Forest Ecology and Management* **46**: 59–102.

Ulanova NG. 2000. The effects of windthrow on forests at different spatial scales: a review. *Forest Ecological Management* **135**: 155–167.

Vedachalam V. 2011. Discrete Element Modelling of Granular Snow Particles using LIGGGHTS. Master's Thesis, The University of Edinburgh.

Viles H. 1988. *Biogeomorphology*. Basil Blackwell: Oxford.

Walton O. 1993. Numerical simulation of inclined chute flows of monodisperse, inelastic, frictional spheres. *Mechanics of Materials* **16**: 239–247.

Wilkinson MT, Richards PJ, Humphreys GS. 2009. Breaking ground: pedological, geological, and ecological implications of soil bioturbation. *Earth-Science Reviews* **97**: 257–272.